J. Fluid Mech. (2007), *vol.* 587, *pp.* 453–469.
doi:10.1017/S0022112007007318 Printed in the United Kingdom

Instability of the buoyancy layer on an evenly heated vertical wall

G. D. McBAIN[1], S. W. ARMFIELD[1] AND GILLES DESRAYAUD[2]

[1]School of Aerospace, Mechatronic Engineering, The University of Sydney, Darlington, NSW 2006, Australia

[2]LETEM Laboratory, INSSET, University of Picardie, 02109 Saint-Quentin, France

(Received 20 December 2006 and in revised form 3 May 2007)

The stability of the buoyancy layer on a uniformly heated vertical wall in a stratified fluid is investigated using both semi-analytical and direct numerical methods. As in the related problem in which the excess temperature of the wall is specified, the basic laminar flow is steady and one-dimensional. Here flows varying in time and with height are considered, the behaviour being determined by the fluid's Prandtl number and a Reynolds number proportional to the ratio of two temperature gradients: the horizontal one imposed at the wall and the vertical one existing in the far field. For low Reynolds numbers, the flow is stable with variation only in the wall-normal direction. For Reynolds numbers greater than a critical value, depending on the Prandtl number, the flow is unstable and supports two-dimensional travelling waves. The critical Reynolds number and other properties have been obtained via linearized stability analysis and are shown to accurately predict the behaviour of the full nonlinear solution obtained numerically for Prandtl number 7. The stability analysis employs a novel Laguerre collocation scheme while the direct numerical simulations use a second-order finite volume method.

1. Introduction

We consider natural convection in a very simple configuration: an extensive fluid with a stable vertical temperature gradient γ_s against a heated vertical wall $x = 0$ (figure 1). If the wall is supposed to have a uniform temperature difference ΔT over the far field, the Oberbeck–Boussinesq equations admit a simple analytic steady solution (Prandtl 1952, pp. 422–425); the flow is parallel to the wall, and it and the excess temperature $T(x, y) - T(\infty, y)$ depend only on the distance x from the wall.

It follows (Shapiro & Fedorovich 2004*b*) that the wall heat flux is uniform, and that the solution also applies when the excess temperature boundary condition is replaced by one of a uniform normal temperature gradient (γ_w, as indicated in figure 1). This flux condition is perhaps more natural, say, as a model of solar radiation (Tao, Le Quéré & Xin 2004*a*) or electrical resistance heating, or of radiative cooling to a clear night sky. It is thus the more natural condition (Manins & Sawford 1979; Skyllingstad 2003) for Prandtl's (1952, pp. 422–425) original problem where (Kolobkov 1960, p. 57)

> At night the ground cools off due to radiation losses into outer space. This cooling is conveyed to the strata of air in direct contact with the ground. But the cooling process is slow and occurs in a thin layer because air is a poor conductor of heat. Besides, at night there are fewer eddy currents in the atmosphere to mix the air.

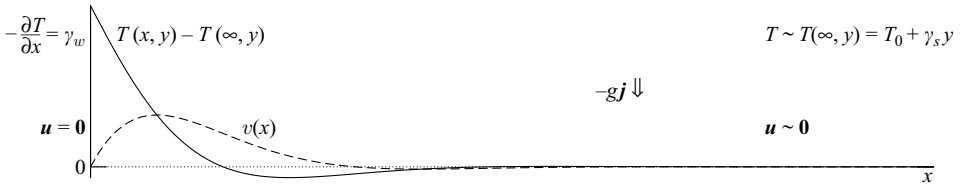

FIGURE 1. Configuration and base flow: stratified fluid with an evenly heated vertical wall. The coordinate x is normal out from the wall, and y is vertical with unit vector $\boldsymbol{j}$.

Unless the ground is horizontal a katabatic wind is generated. Prandtl's solution also arises in a rectangular cavity with evenly heated and cooled vertical walls if the horizontal flux is so strong that the core stratifies and the flow is confined to a boundary layer circulation around the walls (Kimura & Bejan 1984). The mass transfer analogue of this configuration describes electrodeposition, for which again the flux condition is more appropriate than a concentration condition (Eklund *et al.* 1991; Bark, Alavyoon & Dahlkild 1992).

Further, 'a vertical flat plate with a uniform flux boundary condition often is easier to construct and to control in experimentation' (Polymeropoulos & Gebhart 1966). In the related problem when the wall is tilted and even an adiabatic condition at the wall produces flow (Wunsch 1970; Phillips 1970), the (zero) flux condition is trivially engineered in the mass transfer analogue (Peacock, Stocker & Aristoff 2004).

Although the two steady laminar solutions are identical, their stability properties need not be since the temperature perturbations satisfy in the one case a Dirichlet and in the other a Neumann homogeneous boundary condition at the wall. This appears to have been overlooked by Tao *et al.* (2004*a*, *b*) and Tao (2006), who set the temperature perturbation to zero at the wall yet refer to it as a 'uniform-heat-flux boundary condition'. We show that for small and moderate Prandtl numbers, including those corresponding to air and water, the choice of thermal boundary condition makes a significant difference to the stability.

If the steady laminar solutions are attractive, the evolution to them would be different too; this has been studied recently by Shapiro & Fedorovich (2004*a*,*b*) under the restriction that the solution remains one-dimensional throughout. In the present work we relax this restriction and allow two-dimensional variation.

The linear stability of the base solution in the Dirichlet case has been thoroughly treated by Gill & Davey (1969). In this paper, we extend their results to the heat flux condition. To our knowledge, the only previous attempts to do this are of limited availability (Desrayaud, Nguyen & Le Peutrec 1989; Desrayaud & Nguyen 1989; Desrayaud 1990).

Further, as a linear stability analysis provides only sufficient conditions for instability, we supplement it with numerical solutions of the nonlinear two-dimensional evolution equations. At a particular Prandtl number ($Pr = 7$), they show supercritical bifurcation of travelling wave solutions from the steady one-dimensional solution at the Reynolds number, longitudinal wavenumber, and wave speed predicted by the linear theory.

That the bifurcation is supercritical is consistent with other one-dimensional natural convection base flows, namely: the unstratified slot, as demonstrated in numerous studies (Gershuni & Zhukhovitskii 1976; Bratsun, Zyuzgin & Putin 2003); the stratified slot, as shown by the numerical simulations of Christov & Homsy (2001);

and the anabatic wind on a temperature-specified wall, as proven by the weakly nonlinear analysis of Iyer & Kelly (1978).

We also mention the global stability results for the temperature boundary condition case obtained by Joseph (1976). These provided lower bounds on the greatest ΔT for which all disturbances must monotonically decay; however, as the bounds are very conservative and the system (with either boundary condition) bifurcates supercritically at the parameter values predicted by linear stability theory, we do not pursue this approach here.

2. Formulation

With the length and velocity scales used by Gill & Davey (1969),

$$\delta = \left(\frac{4\nu\alpha}{g\beta\gamma_s}\right)^{1/4}, \quad U_{\Delta T} = \Delta T \left(\frac{g\beta\alpha}{\nu\gamma_s}\right)^{1/2} \tag{2.1a, b}$$

(where ν, α, and β are the coefficients of kinematic viscosity, thermal diffusivity, and thermal expansion) the anabatic wind solution of Prandtl (1952, pp. 422–425) with the prescribed wall temperature excess ΔT takes a particularly simple form, free from dimensionless parameters. The corresponding Oberbeck–Boussinesq equations are

$$Re\,\frac{\mathrm{D}\boldsymbol{u}}{\mathrm{D}t} = -Re\nabla p + 2\vartheta\,\boldsymbol{j} + \nabla^2\boldsymbol{u} \tag{2.3a}$$

$$RePr\,\frac{\mathrm{D}\vartheta}{\mathrm{D}t} = -2v + \nabla^2\vartheta \tag{2.3b}$$

$$\nabla\cdot\boldsymbol{u} = 0, \tag{2.3c}$$

where $\boldsymbol{u}$ is the velocity, v its vertical component, ϑ the temperature excess (over the uniform vertical gradient and scaled with ΔT), t the time (scaled with $\delta/U_{\Delta T}$), and p the pressure excess (over the hydrostatic contribution from the background stratification and scaled with $U_{\Delta T}^2$ times the fluid's density). The governing dimensionless parameters are the Reynolds and Prandtl numbers:

$$Re_{\Delta T} \equiv \frac{U_{\Delta T}\delta}{\nu} = \frac{\Delta T}{\nu}\left(\frac{4g\beta}{\nu}\right)^{1/4}\left(\frac{\alpha}{\gamma_s}\right)^{3/4}, \quad Pr \equiv \frac{\nu}{\alpha}. \tag{2.4a, b}$$

On the boundary (in the original formulation of Prandtl 1952 and Gill & Davey 1969), $\boldsymbol{u} = \boldsymbol{0}$ and $\vartheta = 1$, while both $\boldsymbol{u}$ and ϑ decay for large x.

The base anabatic wind solution has p constant,

$$\boldsymbol{u} = \boldsymbol{j}V(x) \equiv \boldsymbol{j}\mathrm{e}^{-x}\sin x, \quad \vartheta = \Theta(x) \equiv \mathrm{e}^{-x}\cos x. \tag{2.5a, b}$$

Since the dimensionless heat flux out of the wall is unity, the same solution and equations apply to the specified even heat flux problem provided ΔT is replaced with $\gamma_w\delta$ in the velocity and temperature scales, where γ_w is the component of temperature gradient normal to the wall, as in figure 1. The length scale δ (2.1*a*) is determined by the stratification and is independent of the wall conditions. The new velocity scale and Reynolds number are

$$U = \gamma_w\left(\frac{4g\beta}{\nu}\right)^{1/4}\left(\frac{\alpha}{\gamma_s}\right)^{3/4}, \quad Re = \frac{2\gamma_w}{Pr\,\gamma_s}. \tag{2.6a, b}$$

The only other change from the specified wall temperature problem is that now

$$\frac{\partial \vartheta}{\partial x} = -1 \tag{2.7}$$

instead of $\vartheta = 1$ at $x = 0$.

3. Linear stability

3.1. *The linear stability equations*

Although no equivalent of Squire's theorem applies to this system (Gill & Davey 1969), our preliminary investigations of three-dimensional disturbances showed that all infinitesimal oblique waves seemed to be damped more strongly than two-dimensional waves, so we focus here on the latter. The two-dimensional linear stability of the base solution is governed by (Gill & Davey 1969):

$$\psi'''' - 2\kappa^2\psi'' + \kappa^4\psi - \mathrm{i}\kappa Re\{(V-c)(\psi'' - \kappa^2\psi) - V''\psi\} + 2\theta' = 0, \tag{3.1a}$$

$$\theta'' - \kappa^2\theta - \mathrm{i}\kappa RePr\{(V-c)\theta - \Theta'\psi\} - 2\psi' = 0. \tag{3.1b}$$

Here the primes denote differentiation with respect to x, and ψ and θ are the Fourier coefficients of the stream-function and temperature perturbations corresponding to streamwise wavenumber κ and speed c. On solving the eigenvalue problem for an eigenvalue c for fixed Re, Pr, and κ, each eigenmode makes a contribution

$$\delta\boldsymbol{u} = 2\mathrm{Re}\{\epsilon \mathrm{e}^{\mathrm{i}\kappa(y-ct)}(-\mathrm{i}\kappa\psi\boldsymbol{i} + \psi'\boldsymbol{j})\} \tag{3.2a}$$

$$\delta\vartheta = 2\mathrm{Re}\{\epsilon\theta \mathrm{e}^{\mathrm{i}\kappa(y-ct)}\}, \tag{3.2b}$$

where ϵ is an undetermined infinitesimal complex amplitude. The boundary conditions are $\psi(0) = \psi'(0) = \psi(\infty) = \theta(\infty) = 0$ and

$$\theta'(0) = 0; \tag{3.3}$$

i.e. similar to those of Gill & Davey (1969) but with (3.3) in place of $\theta(0) = 0$.

Our novel method of discretizing and solving the linear stability problem uses generalized Laguerre collocation and is described in the Appendix.

3.2. *The linear stability margin for $Pr = 7$*

At a given Pr and Re, the flow is unstable with respect to infinitesimal perturbations of real wavenumber κ if any c in the spectrum has a positive imaginary part. Given a point in the Re–κ plane for which this condition holds and another for which it does not, a *marginal* point (at which both κ and the c with greatest imaginary part are real) can be found between the two by bisection.

The marginal curve can then be traced by numerical continuation, as shown in figure 2 for $Pr = 7$. The cusp near $Re = 130$ and $\kappa = 0.53$, representing an exchange of stabilities between two modes as discussed in § 3.3, requires a robust continuation procedure but is easily negotiated by the adaptive skirting algorithm of McBain (2004).

After roughly locating the critical Reynolds number Re_c (the minimum Re on the stability margin), a golden section search (e.g. Greig 1980, p. 37) in κ was used to find $Re_c \doteq 8.58134$ and $\kappa_c \doteq 0.4612$ at $Pr = 7$. The critical mode has phase speed $c_c \doteq 0.3874$ and is illustrated in figure 3.

3.3. *Effect of Prandtl number and thermal boundary condition*

The critical mode was found similarly for many Prandtl numbers between 0 and 10^3, for both the temperature excess and temperature gradient boundary conditions. The

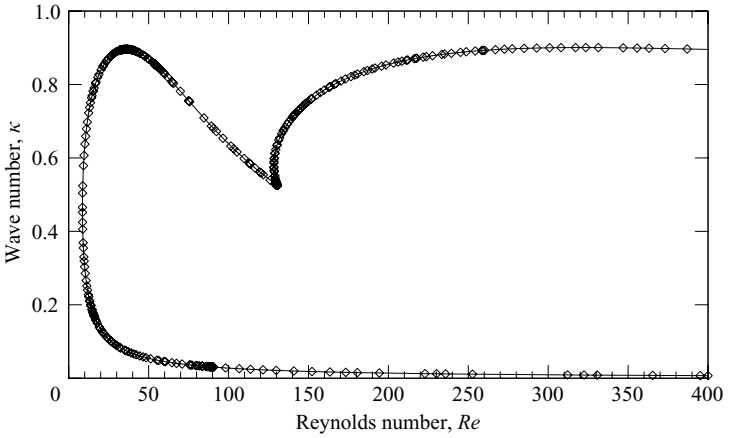

FIGURE 2. The linear stability margin for $Pr = 7$.

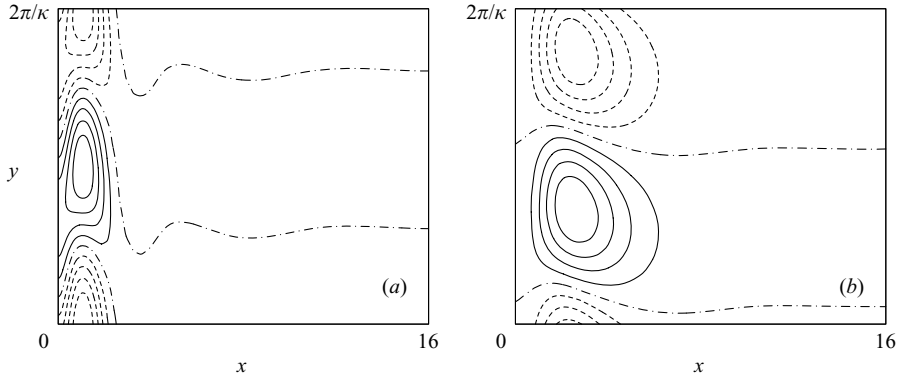

FIGURE 3. (*a*) Isotherms and (*b*) streamlines of one wavelength of the critical mode for $Pr = 7$ ($Re_c = 8.58134$, $\kappa_c = 0.4612$, $c_c = 0.3874$). The levels are equally spaced, though the amplitude is indeterminate; the solid, chain, and dashed lines mark positive, zero, and negative levels.

critical Reynolds numbers and corresponding wave speeds are plotted in figure 4(*a*,*b*) along with the data of Gill & Davey (1969) for the temperature condition and Desrayaud (1990) for the heat flux condition. Both previous studies are consistent with the present work.

While broad qualitative similarities are apparent between the results for the different thermal boundary conditions, one can also distinguish systematic differences, which in some important places are quantitatively significant.

In both the Dirichlet and Neumann cases in figure 4(*a*) Re_c (i): is constant for small Pr; (ii) decreases and then increases; (iii) to a cusp; (iv) then decays rapidly with increasing Pr; and finally (v) goes like $Pr^{-1/2}$ as $Pr \to \infty$, the asymptote here being that derived by Gill & Davey (1969). Correspondingly, the critical wave speed in figure 4(*b*): (i) is constant and less than the peak velocity V_{max} of the base flow, marked with a dashed line in figure 4(*b*); (ii) slowly increases; (iii) jumps closer to V_{max}; (iv) increases past it; and eventually (v) levels off.

The differences are that: (i, ii) the heat flux condition is stabilizing at low Prandtl numbers with Re_c 20–30% higher; (iii) the discontinuity is at a lower Pr, 0.22 vs.

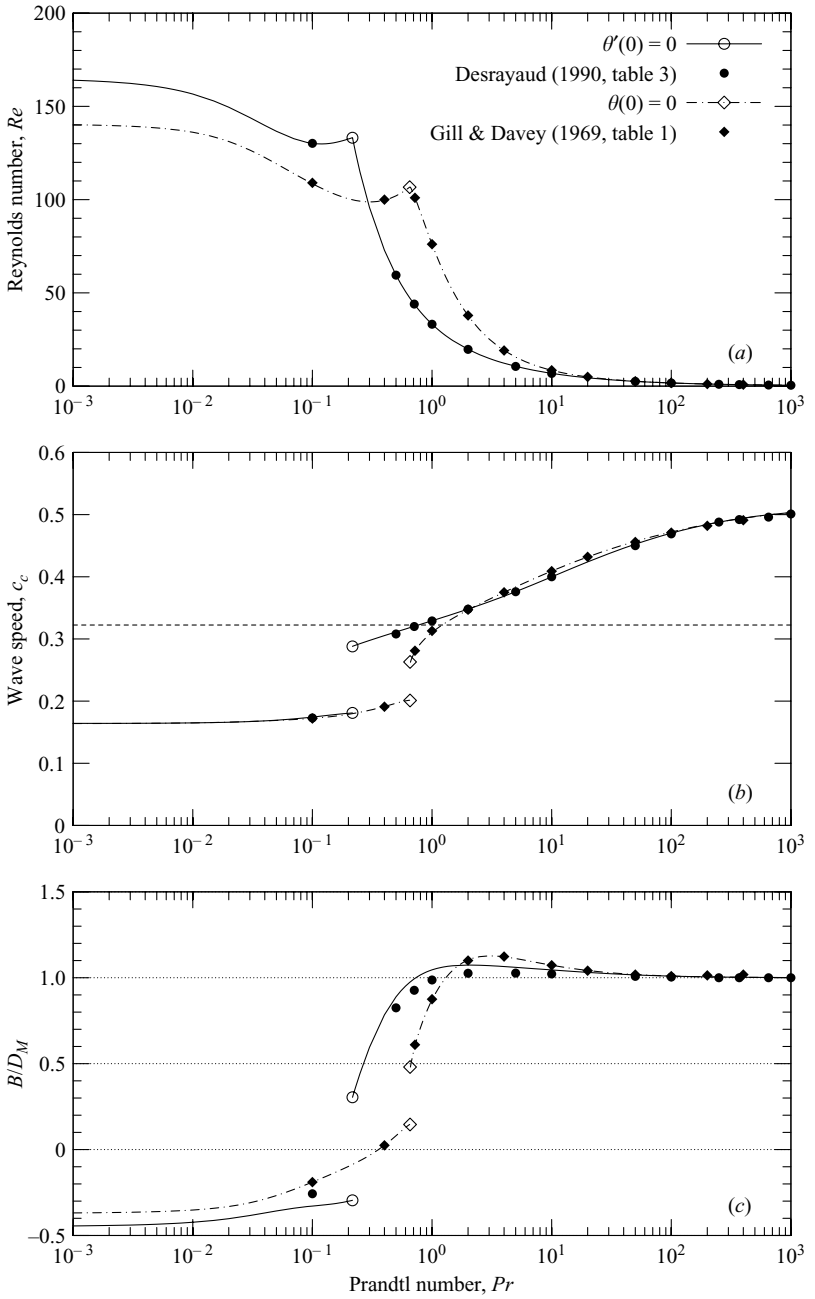

FIGURE 4. (*a*) Reynolds number, (*b*) speed, and (*c*) relative buoyant production of the critical mode for even heating (solid curve) or excess temperature (chain). Open points mark discontinuities; solid points are from previous studies as marked.

0.65; (iv) the heat flux condition is destabilizing just beyond the cusp with Re_c less than half that for the Dirichlet condition. As $Pr \to \infty$, (v), the Neumann and Dirichlet cases become indistinguishable.

3.3.1. *Kinetic energy and its buoyant production and viscous dissipation*

Following Gill & Davey (1969) and Iyer (1973), the Pr effects can be interpreted in terms of the balance for the kinetic energy of the disturbance:

$$\kappa Re E_M \mathrm{Im} c = -D_M + Re\, M + B \tag{3.4}$$

where (using a star to denote a complex conjugate)

$$E_M \equiv \int_0^\infty \psi^*(\kappa^2\psi - \psi'')\,\mathrm{d}x, \tag{3.5a}$$

$$D_M \equiv \int_0^\infty \psi^*(\kappa^4\psi - 2\kappa^2\psi'' + \psi'''')\,\mathrm{d}x, \tag{3.5b}$$

$$M \equiv -\kappa\,\mathrm{Im}\int_0^\infty \psi^* V \psi''\,\mathrm{d}x, \tag{3.5c}$$

$$B \equiv -2\mathrm{Re}\int_0^\infty \psi^*\theta'\,\mathrm{d}x; \tag{3.5d}$$

different but equivalent definitions are given by Gill & Davey (1969).

For a marginally stable disturbance, $\mathrm{Im}\, c = 0$ so that the disturbance kinetic energy E_M drops out of the balance (3.4), and, following Iyer (1973) in normalizing by the rate of viscous dissipation D_M, we obtain

$$0 = -1 + Re\,\frac{M}{D_M} + \frac{B}{D_M}. \tag{3.6}$$

Since B is the rate of production of disturbance kinetic energy by buoyancy forces, we call B/D_M the *relative buoyant production*. If this ratio exceeds one-half, the mode is *buoyancy-driven* (Iyer 1973); if it were unity, all the energy would be due to buoyancy, which is the case for large Prandtl numbers. When the ratio is negative, thermal effects retard the instability. The critical-mode relative buoyant production is plotted across the Prandtl number range in figure 4(c). For either boundary condition, it may be seen that the discontinuity in the critical mode as the Prandtl number increases is from a hydrodynamically driven to a buoyancy-driven mode. This is to be expected, given that the same phenomenon occurs for the boundary layer on an isothermal plate in an isothermal fluid (Nachtsheim 1963), in unstratified (Birikh *et al.* 1972; Chen & Perlstein 1989; McBain & Armfield 2004) and stratified (Bergholz 1978) vertical slots, as well as in the Dirichlet case (Gill & Davey 1969).

What is new is the effect of the boundary conditions. In general, compared to the excess temperature condition, the heat flux condition is 'less restrictive' on the temperature field. This relation between eigenvalue problems with Neumann and Dirichlet conditions is very common. For example, it is well known that the eigenvalues of $-\nabla^2$ are lower for Neumann than Dirichlet conditions (Levine & Weinberger 1986, for example). Familiar physical examples of the phenomenon include the pitches of struck bars with free and fixed ends (e.g. Morley 1954, p. 484), the buckling strength of pivoted and built-in beams (e.g. Morley 1954, pp. 291–296), or the critical Rayleigh numbers of unstably stratified vertical tubes with insulating and perfectly conducting walls (Gershuni & Zhukhovitskii 1976, p. 60). Thus, for small Pr, when thermal effects are retarding the disturbance ($B < 0$), this thermal effect is enhanced, the system is stabilized, and Re_c increased. Similarly, the second mode, which is buoyancy-driven, i.e. dependent on a disturbance of the temperature field, sets in more readily, and takes over from the hydrodynamically driven first mode at a lower Prandtl number.

That the two cases coalesce as $Pr \to \infty$ is obvious from the asymptotic analysis of Gill & Davey (1969): in the limit, the second-order conduction term disappears from the temperature equation and the wall boundary condition has to be dropped. Moreover, the results (Gill & Davey 1969, figure 11) show that the thermal disturbance is localized away from the wall.

3.3.2. *Summary comparison of flux and temperature excess conditions*

So for large Prandtl numbers, the Neumann and Dirichlet problems coincide, whereas for small Prandtl numbers, the thermal boundary condition does matter. This is because, for either wall condition, even in the $Pr \to 0$ limit, the hydrodynamic stability problem does not become independent of the temperature, as it does for the unstratified slot (Birikh 1966) and isothermal semi-infinite plate (Plapp 1957; Szewcyzk 1962; Kurtz & Crandall 1962; Nachtsheim 1963). Buoyancy is always important. This difference between the half-space and the slot arises because the length scale δ (2.1) depends on the thermal diffusivity. If the stability problem were independent of buoyancy, the thermal boundary condition would be irrelevant.

The most notable consequence of the change to the heat flux condition is that the primary buoyancy-driven mode is destabilized, taking over from the primary hydrodynamically driven mode as the critical mode at a lower Prandtl number, and becoming unstable at lower Reynolds numbers for Pr just above this. This range of Pr includes the practically important values $Pr = 0.7$ (typical of air), for which the critical Reynolds number drops 57% from 103.1 to 48.5, and $Pr = 7$ (typical of water), for which it drops 25% from 11.5 to 8.6. Clearly, using the appropriate thermal boundary condition will have a significant quantitative effect in practical problems.

4. Direct simulation for $Pr = 7$

Using a second-order fractional step Navier–Stokes solver on a non-staggered rectangular grid (Armfield & Street 1999, 2002, 2003), (2.3) was solved in the domain $0 \leqslant x \leqslant X$, $0 \leqslant y \leqslant Y$ with initial conditions $\boldsymbol{u} = \boldsymbol{0}$ and $\vartheta = 0$, subject to wall conditions $\boldsymbol{u} = \boldsymbol{0}$ and (2.7) at $x = 0$, truncated far-field conditions

$$\frac{\partial u}{\partial x} = v = \frac{\partial \vartheta}{\partial x} = 0 \qquad \text{at } x = X, \tag{4.1}$$

and periodic conditions on $\boldsymbol{u}$ and ϑ at $y = 0$ and $y = Y$.

Results were obtained on a domain with $X = 16$ and $Y = 2\pi/\kappa = 2\pi/0.454 = 13.84$, using a uniform grid of 55 steps in the y-direction, and a grid of 116 steps lengthening geometrically with common ratio 1.025 in the x-direction, giving a smallest step of 0.0248 across $x = 0$. The time step used was $\Delta t = 0.0005$. The y-wavenumber $\kappa = 0.454$ of the domain was chosen to match that of the most unstable mode at $Re = 9$, slightly above the critical value $Re_c \doteq 8.58134$ at $Pr = 7$. The linear marginal Reynolds number at this wavenumber is $Re_m = 8.584$, which is close to the critical value, as expected from the flatness of Re_m near its minimum in figure 2.

For small enough Re the fully developed solution is expected to match the analytical solution (2.5). The numerical solution for $Re = 8.5\,(< Re_m)$ was found to have achieved a fully developed steady state by time $t = 1000$. The fully developed x-profiles of velocity and temperature agree with the analytical solution to within ± 0.002 at any node, demonstrating that the domain and grid are suitable for the base flow.

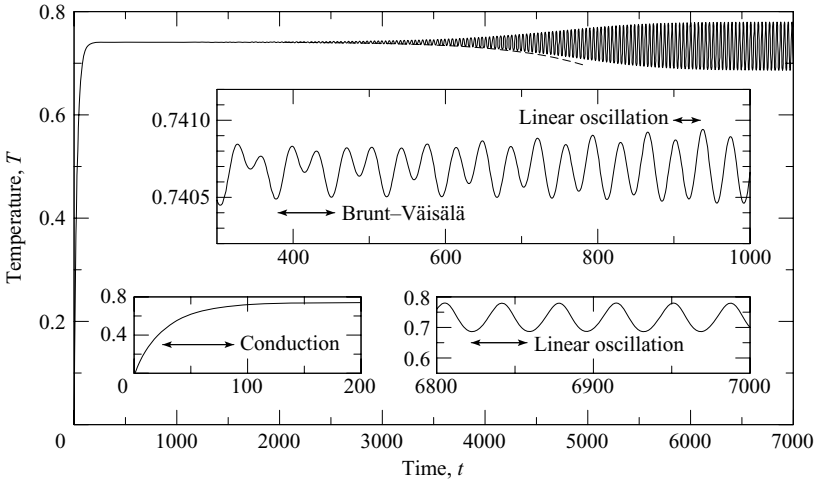

FIGURE 5. Temperature history ($x = 0.264$, $Re = 9$, $Pr = 7$), with dashed line marking linear stability growth-rate envelope and insets showing the conduction time scale $RePr$, the Brunt–Väisälä period $\pi RePr^{1/2}$, and the linear stability oscillation period $2\pi/\kappa \mathrm{Re}\, c$.

Results were then obtained for $Re = 9\,(> Re_m)$; a temperature signal at an arbitrary point ($x = 0.264$) is presented in figure 5. As can be seen, the fully developed flow is now time-periodic. Grid convergence, time step, and domain size tests have been carried out to confirm that the solution is in the asymptotic region for this grid and time step, and that the influence of the $x = X$ boundary (4.1) is not significant. The influence of the $y = Y$ boundary, which restricts the wavenumbers that can be present in the solution, was assessed by obtaining results for $5 \leqslant Y \leqslant 100$; the unresolved modes for the $Y = 13.84$ case are not significant, in all cases the wavelength 13.84 was found to be dominant.

The development for this flow is shown in insets to figure 5, where the initially multimodal signal evolves into a single mode via the decay of stable modes and the growth of the linearly unstable mode. Assuming the initial phase is controlled by one-dimensional transient thermal conduction, i.e. that capacity balances conduction in (2.3 *b*), we expect a time scale $O(RePr)$; this is consistent with the signal in figure 5, for which $RePr = 63$. Although the solution depicted gradually becomes two-dimensional, the early stages are essentially one-dimensional, as in the analysis of Shapiro & Fedorovich (2004*b*), and the time scale $O(RePr)$ is consistent with their figure 5, for example (noting that it corresponds to a time scale of Pr in their units). Also evident around $t = 400$ are Brunt–Väisälä oscillations (resulting from capacity–stratification and inertia–buoyancy balances in the one-dimensional governing equations) with characteristic period $\pi RePr^{1/2} \doteq 74.8$.

After the decay of the initial transients, the numerical solution behaves very much as predicted by linear stability theory. In the period $2000 < t < 5000$, numerical signal processing gives the growth rate as 0.001370 and the dominant frequency as 0.0275, whereas the results predicted using the linear stability method of § 3 for the fastest growing mode at the same Reynolds and Prandtl numbers, and wavenumber are $\kappa \mathrm{Im}\, c = 0.001372$ and $\kappa \mathrm{Re}\, c/2\pi = 0.02797$. The discrepancies are within 0.2% and 2%, respectively, showing that the nonlinear effects that eventually limit the growth have only a small effect on the time-behaviour of the most unstable mode, and that the numerical solution accurately resolves the evolution.

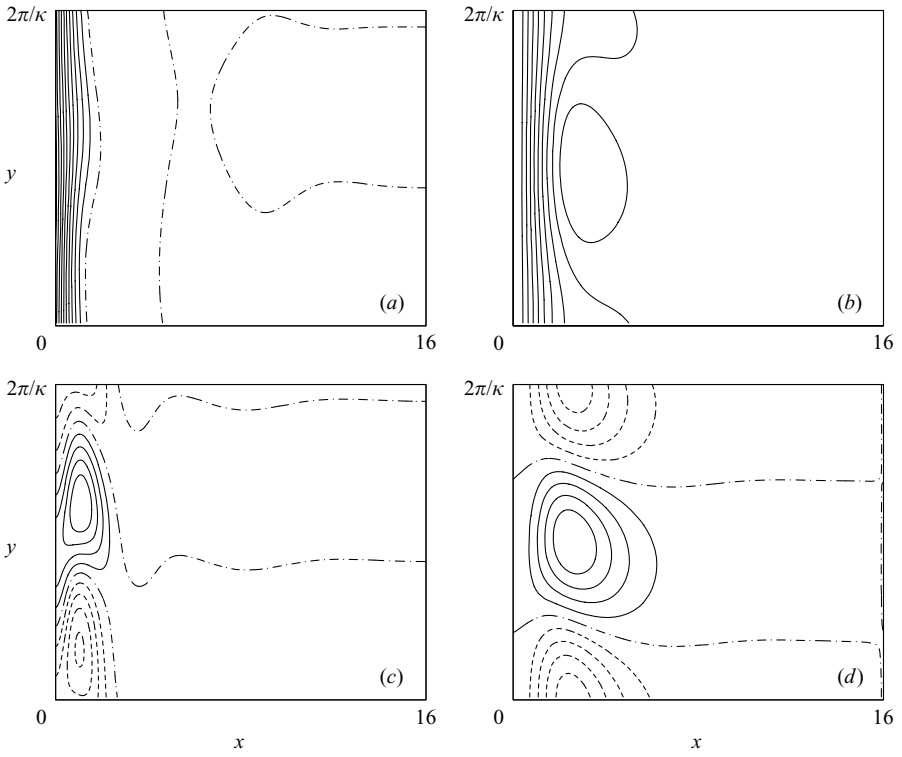

FIGURE 6. (a, c) Isotherms and (b, d) streamlines for the $Re = 9$ case; (a, b) total and (c, d) difference from streamwise mean. Levels at (a) 0(0.1)1, (b) $0.0191 \times -4(1)4$, (c) $0.0596 \times 1(1)9$, and (d) $0.01545 \times -4(1)5$. Line styles as figure 3.

The final unsteady flow consists of waves travelling vertically; that is, up the natural convection boundary layer that has formed on the heated wall. Figure 6 contains the isotherms and streamlines for the $Re = 9$ solution, where the wave structure is clearly seen in both the temperature and velocity fields. The wavelength is equal to the vertical extent of the domain and the wave speed is 0.38 – approximately the same as the real part of the speed $c = 0.387 + 0.00302\mathrm{i}$ of the fastest growing mode of linear theory. We also plot the difference between the solution and its streamwise mean for easier comparison with the critical mode of the linear theory (figure 3).

Finally, a solution was obtained at a much higher Reynolds number, $Re = 20$; figure 7 contains the temperature and stream-function contours, again showing the travelling wave although with considerably increased amplitude and modified structure – a sharper peak faces upstream. The modified structure is a result of nonlinear effects. Nonlinear effects limit the growth of the primary unstable linear mode by modifying the mean flow and by transferring energy to harmonics that are, in a linear sense, stable (Stuart 1958). The effect on the mean flow can be seen in figure 8, where the vertical-mean temperature and velocity profiles are presented for the two cases with $Re > Re_m$. The $Re = 9$ and base analytical results are seen to be very close, indicating that nonlinear effects lead to only a small modification of the base flow at this Reynolds number. The $Re = 20$ result shows a much larger variation with respect to the base flow, with the temperature at the wall and the peak velocity

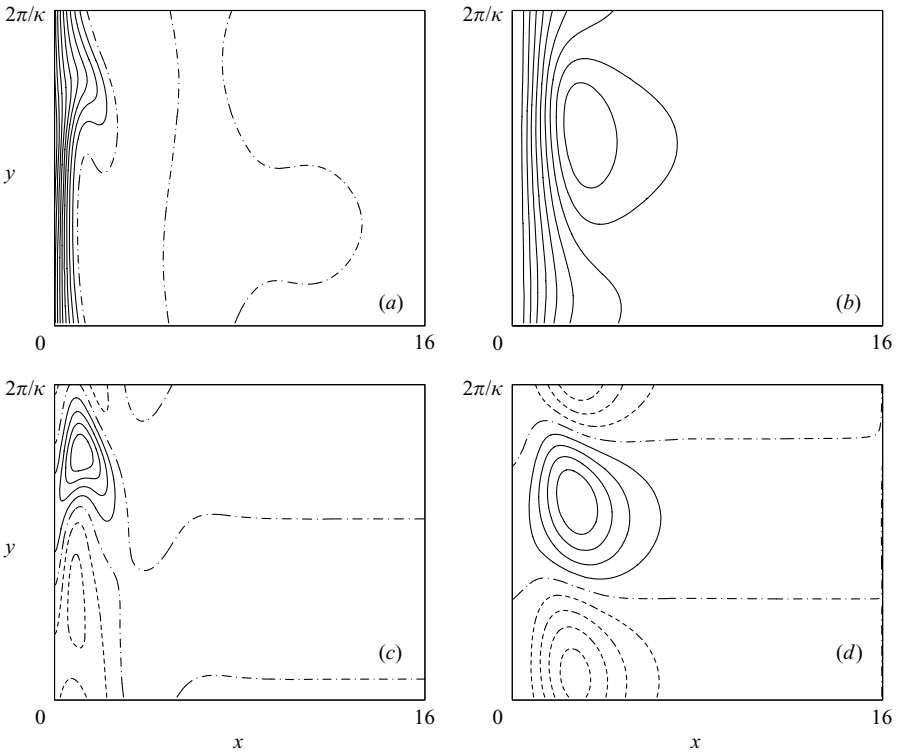

FIGURE 7. As figure 6 but for $Re = 20$; levels at (*a*) 0(0.1)1, (*b*) $0.0646 \times 1(1)9$, (*c*) $0.05628 \times -2(1)4$, and (*d*) $0.0256 \times -4(1)4$.

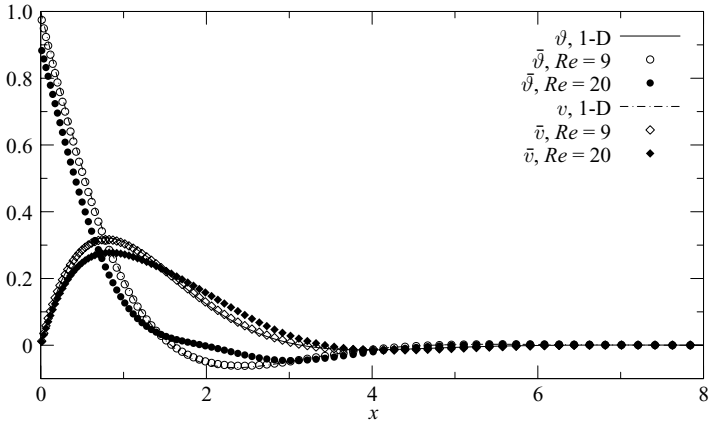

FIGURE 8. Vertical mean profiles of excess temperature $\bar{\vartheta}$ (circles) and vertical velocity $\bar{v}$ (diamonds) for $Re = 9$ (open) and 20 (solid); curves also plotted for the analytical steady one-dimensional solution (2.5).

both about 10% lower, while the temperature and velocity in the outer region of the boundary layer are both higher. The effect of the waves is evidently to increase the effectiveness of heat and momentum transfer from the inner to the outer region of the boundary layer.

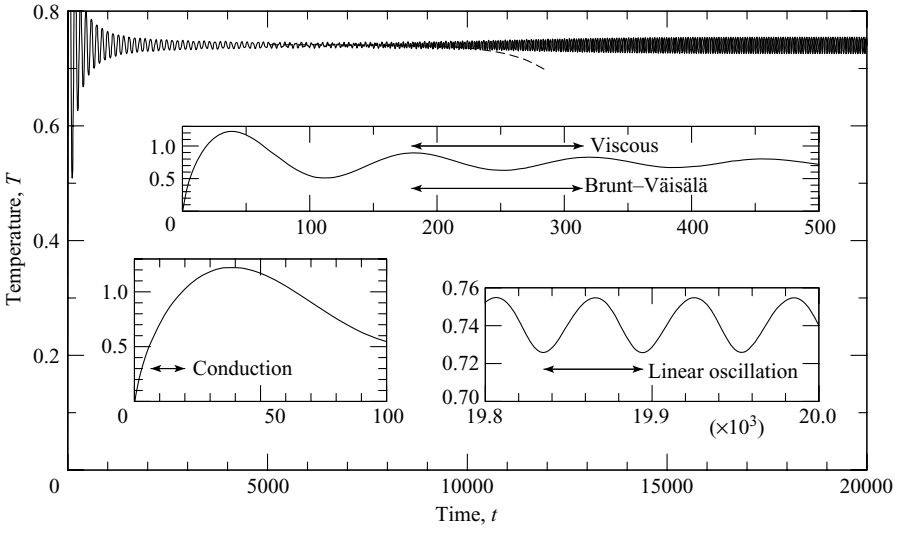

FIGURE 9. Temperature history ($x = 0.264$, $Re = 135$, $Pr = 0.1$); insets show the conduction time scale $RePr$, the Brunt–Väisälä period $\pi RePr^{1/2}$, and the linear stability oscillation period $2\pi/\kappa \mathrm{Re}\, c$; dashed line marks linear stability growth-rate envelope.

4.1. *Direct simulation at a low Prandtl number, $Pr = 0.1$*

Noting that the system admits two critical modes, depending on the Prandtl number, another simulation was carried out at $Pr = 0.1$. The Reynolds number was chosen as $Re = 135$, again slightly higher than the critical value ($Re = 108.5$). The temperature signal at a point is plotted in figure 9. Again the unstable oscillation predicted by linear stability analysis appears, grows at the predicted rate, and then saturates.

This simulation also demonstrates the three time scales mentioned above: the early conduction–capacity time $RePr = 13.5$; the Brunt–Väisälä oscillation period $\pi RePr^{1/2} = 134.1$; and the linear stability oscillation period $2\pi/\kappa \mathrm{Re}\, c \doteq 59.5$. In addition, for $Pr < 1$, the lower viscosity leads to underdamping and an overshoot in the initial one-dimensional development (Shapiro & Fedorovich 2004*a*) decaying over a viscous–inertial balance time of order $Re = 135$, which is evident in the period $0 < t < 500$ in figure 9. Although this viscous decay time scale happens to be close to the Brunt–Väisälä period in this example (as $\pi Pr^{1/2} \doteq 0.99$), the two effects are easily distinguished since the Brunt–Väisälä oscillations are non-dissipative in origin.

4.2. *Heat transfer rate and temperature difference*

A single measure of the effect of the travelling waves is the Nusselt number, defined as the mean ratio of the local heat transfer coefficient

$$h \equiv \frac{k\gamma_w}{T|_{x=0} - T|_{x\to\infty}} = \frac{k}{\vartheta|_{x=0}\delta} \tag{4.2}$$

(where k is the fluid thermal conductivity) to that prevailing everywhere under the base flow $h_0 = k/\delta$; i.e.

$$Nu \equiv \frac{\kappa}{2\pi}\int_0^{2\pi/\kappa} \frac{h}{h_0}\,\mathrm{d}y = \frac{\kappa}{2\pi}\int_0^{2\pi/\kappa} \frac{\mathrm{d}y}{\vartheta|_{x=0}}. \tag{4.3}$$

As seen in figure 8, the travelling waves have the effect of increasing the heat transfer away from the wall and thereby decreasing the temperature at the wall, which will

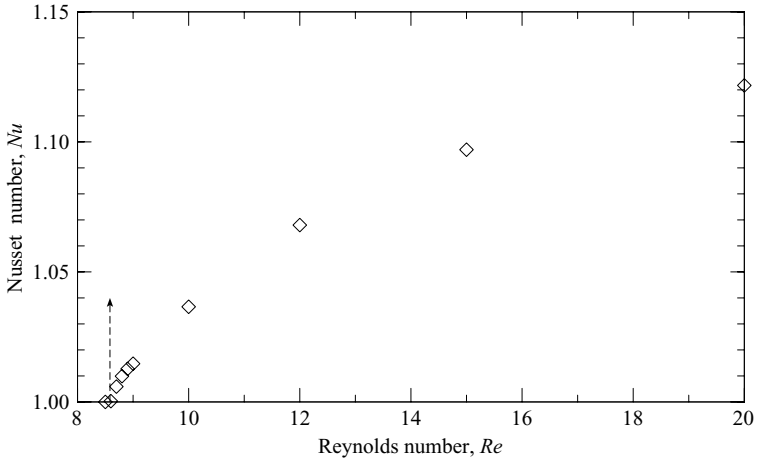

FIGURE 10. Nusselt number versus Re for $\kappa = 0.454$; arrow: linear theory ($Re_m = 8.584$); points: direct numerical simulation.

lead to a Nusselt number greater than one. Nusselt numbers obtained for a range of Reynolds numbers at $Pr = 7$ and $\kappa = 0.454$ are shown in figure 10. The figure provides an approximation for Re_m of slightly greater than 8.5, corresponding closely to the linear marginal value 8.584.

5. Concluding discussion

Prandtl's exact steady one-dimensional solution of the Oberbeck–Boussinesq equations for a buoyancy layer on a vertical wall in a stably stratified fluid holds not only for the boundary condition in which the wall temperature increases linearly with altitude at the same rate as the far-field stratification, but also for the more realistic uniform heat flux condition. We have studied the stability of this system with respect to two-dimensional vertically periodic disturbances.

Using generalized Laguerre collocation for infinitesimal disturbances, we determined the linear stability margin, the critical Reynolds number, and the critical wave mode for Prandtl numbers from zero to 10^3. The linear stability results are qualitatively similar to those for the specified temperature excess problem, though there are notable systematic differences which were explained with reference to the disturbance kinetic energy balance and which are particularly quantitatively significant in the practically important range of Prandtl numbers including air and water.

Direct simulation has been used to obtain full solutions to the governing equations for $Pr = 7$, a fixed streamwise wavenumber $\kappa = 0.454$ close to the critical value $\kappa_c = 0.4612$, and a set of Reynolds numbers spanning the associated linear marginal value $Re_m = 8.584$. Plotting the Nusselt number against Reynolds number for the numerical results showed that the nonlinear system bifurcates supercritically and the plot provides a good approximation of the marginal Reynolds number.

A detailed comparison of the direct simulation and stability analysis results was carried out for $Re = 9$, showing that the simulation and stability analysis produce nearly identical results for the frequency and growth rate.

It is noted that a vertical length scale is imposed on the direct simulation solution by the height $Y = 2\pi/\kappa$ of the domain. For the results presented this was chosen to correspond to the most unstable wavelength obtained from the stability analysis for

$Re = 9$. The simulation can then only contain modes with wavenumber $\ell\kappa$, for integer ℓ up to half the number of vertical grid steps. Results have also been obtained for other domain heights to ensure that unresolved modes for the $2\pi/\kappa = 13.84$ case are not significant; in all cases at $Re = 9$ the wavelength 13.84 was found to be dominant.

The full numerical results show that the nonlinear effects, which eventually limit the amplitude of the unstable mode, only slightly distort the shapes of the base flow and the first harmonic at $Re = 9$. This indicates that results from linear stability analysis can be expected to provide a good representation of the flow structure and behaviour over some range of Re beyond the marginal value. The semi-analytical stability code is 10^5–10^6 times more computationally efficient than the direct simulation code, and may therefore be used far more effectively in large-scale studies of the behaviour of flows of the type considered here.

G. D. M. and S. W. M. acknowledge funding from The University of Sydney's Sesqui Postdoctoral Fellowship scheme and the Australian Research Council's Discovery scheme, respectively. We thank one of the reviewers for noticing the presence of the Brunt–Väisälä frequency in the temperature history of figure 5 and for suggesting the additional run at $Pr = 0.1$.

Appendix. Numerical solution of the linear stability equations

A.1. *Discretization*

The system (3.1) was discretized with ordinate-based interior collocation (Frazer, Duncan & Collar 1938; Villadsen & Stewart 1967). As in our linear stability study of the slot (McBain & Armfield 2004), the method closely follows that of Weideman & Reddy (2000) for the Orr–Sommerfeld equation. That is, the general term $a(x)f^{(k)}(x)$ is discretized as $\sum_j a_i D^k_{ij} f_j$, where fields are represented by a column of ordinates at n collocation points x_i, e.g. $a_i = a(x_i)$, and the 'differentiation matrices' are

$$D^k_{ij} = \sum_{m=0}^{k} \binom{k}{m} \frac{\beta^{(k-m)}(x_i)}{\beta(x_j)} l^{(m)}_j(x_i). \tag{A 1}$$

Here the $l_j(x)$ are the polynomials of degree $n-1$ with the property that $l_j(x_i) = \delta_{ij}$ and $\beta(x)$ is chosen to enforce the boundary conditions.

Here we introduce two modifications: in the choice of the collocation points and in the treatment of the homogeneous Neumann boundary condition (3.3).

A.2. *Gauss–Laguerre–Radau points*

For boundary value problems on $0 \leqslant x < \infty$, Weideman & Reddy (2000) use the roots of the Laguerre polynomial

$$L_n(x) = L^{(0)}_n(x). \tag{A 2}$$

Collocation points should generally be chosen as the abscissae of a Gaussian quadrature rule (Boyd 2001, ch. 4; though we note this has been queried by Fornberg 1996, ch. 4). In the Gauss–Laguerre–Radau quadrature rule (Davis & Rabinowitz 1984, pp. 223–224), these are the roots of the generalized Laguerre polynomial $L^{(\alpha+1)}_n(x)$ which means (A 2) corresponds to $\alpha = -1$, but the generalized Laguerre polynomials are only defined for $\alpha > -1$, so that there is no rule corresponding to the roots of (A 2).

We therefore choose instead the roots of $L^{(\alpha+1)}_n(x)$ with $\alpha > -1$, in particular $\alpha = -\frac{1}{2}$, which corresponds to a weight function $x^{-1/2}\mathrm{e}^{-x}$ in the orthogonality relation with an inverse square-root singularity at the wall, just as for Chebyshev polynomials

(Hochstrasser 1965, p. 774). Methods for computing Gauss–Laguerre–Radau points have been described by Gautschi (1994) and Laurie (2001).

A.3. *Homogeneous Neumann condition for collocation*

A new method for treating the homogeneous Neumann condition $f'(0)=0$ in interior collocation methods is derived here, based on the derivation of Hermite's interpolation formula (Fröberg 1965, pp. 146–148). For collocation on the zeros of a polynomial $\varpi(x)$, Lagrange's fundamental polynomials (Fröberg 1965, pp. 142–143) are $l_j(x)=\varpi(x)/(x-x_j)\varpi'(x_j)$. Say we attempt to modify a set of basis functions $\phi_j(x)=\beta(x)l_j(x)/\beta(x_j)$ already containing one coercion factor so that they satisfy (3.3) by using another coercion factor:

$$\widetilde{\phi}_j(x)=\frac{\nu_j(x)}{\nu_j(x_j)}\phi_j(x)=\frac{\nu_j(x)}{\nu_j(x_j)}\frac{\beta(x)}{\beta(x_j)}l_j(x). \tag{A 3}$$

This satisfies $\widetilde{\phi}'_j(0)=0$ provided

$$\frac{\nu'_j(0)}{\nu_j(0)}=-\frac{\phi'_j(0)}{\phi_j(0)}. \tag{A 4}$$

The simplest solution is the linear coercion factor

$$\nu_j(x)\equiv x-\frac{\phi_j(0)}{\phi'_j(0)}. \tag{A 5}$$

Differentiating the modified basis functions d times gives

$$\widetilde{\phi}^{(d)}_j(x)=d\frac{k_0+x_j^{-1}}{k_0x_j}\phi^{(d-1)}_j(x)+\frac{(k_0+x_j^{-1})x-1}{k_0x_j}\phi^{(d)}_j(x) \tag{A 6}$$

where

$$k_0\equiv\frac{\varpi'(0)}{\varpi(0)}+\frac{\beta'(0)}{\beta(0)}. \tag{A 7}$$

The differentation matrices $D^d_{ij}=\phi^{(d)}_j(x_i)$ can be computed using the algorithm of Weideman & Reddy (2000), and then combined according to (A 6) to obtain the differentiation matrices incorporating the homogeneous Neumann boundary condition (3.3). This requires, however, the constant k_0, which depends on the choice of the collocation points and the first coercion function $\beta(x)$.

Here, where $\varpi(x)=-L^{(\alpha)}_{n+1}(x)$ and $\beta(x)=\mathrm{e}^{-x/2}$ (to enforce decay for large x), the constant k_0 defined in (A 7) is

$$k_0=-\frac{n+1}{\alpha+1}-\frac{1}{2}. \tag{A 8}$$

A.4. *Implementation*

The above collocation method gives a generalized eigenvalue problem of the form $Lq=cMq$ for eigenvalue c, which we convert to $M^{-1}Lq=cq$ and solve by a standard QR algorithm (Anderson *et al.* 1999; Eaton 2002).

The collocation method as described contains three parameters: the number of interior collocation points n, the generalized Laguerre α, and a length scale ℓ; the last arises since $f_\ell(x)=x/\ell$ for $\ell>0$ is an automorphism on the domain $0\leqslant x<\infty$ and so can be applied to the collocation rules. Here we chose $\ell\approx0.2$ (to move the nodes closer to the wall) and, as noted above, $\alpha=-\frac{1}{2}$, and determined n by first by reproducing the results in table 1 of Gill & Davey (1969), and then by observing

the change in the c of greatest imaginary part with increasing n at $Pr = 7$, $Re = 9$, and $\kappa = 0.454$. The error decreases exponentially for n up to about 60–70 and then slowly increases again; 64 points were used in subsequent computations. Coded in *GNU Octave* (Eaton 2002) and run on a 1.6 GHz Intel Pentium IV, the algorithm takes about 0.35 s to compute the c spectrum for given Pr, Re, and κ.

REFERENCES

Anderson, E., Bai, Z., Bischof, C., Blackford, S., Demmel, J., Dongarra, J., Du Croz, J., Greenbaum, A., Hammarling, S., McKenney, A. & Sorenson, D. 1999 *LAPACK Users' Guide*, 3rd edn. SIAM.

Armfield, S. W. & Street, R. 1999 The fractional-step method for the Navier–Stokes equations on staggered grids: The accuracy of three variations. *J. Comput. Phys.* **153**, 660–665.

Armfield, S. W. & Street, R. 2002 An analysis and comparison of the time accuracy of fractional-step methods for the Navier–Stokes equations on staggered grids. *Intl J. Numer. Meth. Fluids* **38**, 255–282.

Armfield, S. & Street, R. 2003 The pressure accuracy of fractional-step methods for the Navier–Stokes equations on staggered grids. *ANZIAM J.* **44**, C20–C39.

Bark, F. H., Alavyoon, F. & Dahlkild, A. A. 1992 On unsteady free convection in vertical slots due to prescribed fluxes of heat and mass at the vertical walls. *J. Fluid Mech.* **235**, 665–689.

Bergholz, R. F. 1978 Instabilities of steady natural convection in a vertical fluid layer. *J. Fluid Mech.* **84**, 743–768.

Birikh, R. V. 1966 On small perturbations of a plane parallel flow with cubic velocity profile. *J. Appl. Math. Mech.* **30**, 432–438.

Birikh, R. V., Gershuni, G. Z., Zhukhovitskii, E. M. & Rudakov, R. N. 1972 On oscillatory instability of plane–parallel convective motion in a vertical channel. *J. Appl. Math. Mech.* **36**, 707–710.

Boyd, J. P. 2001 *Chebyshev and Fourier Spectral Methods*, 2nd edn. Dover.

Bratsun, D. A., Zyuzgin, A. V. & Putin, G. F. 2003 Non-linear dynamics and pattern formation in a vertical fluid layer heated from the side. *Intl J. Heat Fluid Flow* **24**, 835–852.

Chen, Y.-M. & Perlstein, A. J. 1989 Stability of free-convection flows of variable-viscosity fluids in vertical and inclined slots. *J. Fluid Mech.* **198**, 513–541.

Christov, C. I. & Homsy, G. M. 2001 Nonlinear dynamics of two-dimensional convection in a vertically stratified slot with and without gravity modulation. *J. Fluid Mech.* **430**, 335–360.

Davis, P. J. & Rabinowitz, P. 1984 *Methods of Numerical Integration*, 2nd edn. Academic.

Desrayaud, G. 1990 Stability of flow near a heat-flux plate and comparison with numerical simulations in a square cavity. Report 1990/LT/01. CNAM.

Desrayaud, G. & Nguyen, T. H. 1989 Instabilités thermonconvectives dans une cavité à flux imposés. In *Comptes Rendus. Douzième Congrès Canadien de Mécanique Appliquée* (ed. M. A. Erki & J. Kirkhope), vol. 2, pp. 716–717. Carleton University.

Desrayaud, G., Nguyen, T. H. & Le Peutrec, Y. 1989 Stability of a buoyancy-layer. In *Natural Convection in Enclosures, Eurotherm Seminar No. 11, Extended Abstracts* (ed. G. L. Quarini & G. Lauriat), pp. 67–69. Eurotherm.

Eaton, J. W. 2002 *GNU Octave Manual*. Network Theory.

Eklund, A., Alavyoon, F., Simonsson, D., Karlsson, R. I. & Bark, F. H. 1991 Theoretical and experimental studies of free convection and stratification of electrolyte in a copper refining cell. *Electrochim. Acta* **36**, 1345–1354.

Fornberg, B. 1996 *A Practical Guide to Pseudospectral Methods*. Cambridge University Press.

Frazer, R. A., Duncan, W. J. & Collar, A. R. 1938 *Elementary Matrices and Some Applications to Dynamics and Differential Equations*. Cambridge University Press.

Fröberg, C.-E. 1965 *Introduction to Numerical Analysis*. Addison-Wesley.

Gautschi, W. 1994 Algorithm 726: ORTHPOL – a package of routines for generating orthogonal polynomials and Gauss-type quadrature rules. *ACM Trans. Math. Software* **20**, 21–62.

Gershuni, G. Z. & Zhukhovitskii, E. M. 1976 *Convective Stability of Incompressible Fluids*. Israel Program for Scientific Translations.

Gill, A. E. & Davey, A. 1969 Instabilities of a buoyancy driven system. *J. Fluid Mech.* **35**, 775–798.

Greig, D. M. 1980 *Optimisation*. Longman.

Hochstrasser, U. W. 1965 Orthogonal polynomials. In *Handbook of Mathematical Functions* (ed. M. Abramowitz & I. Stegun), chap. 22, pp. 771–802. Dover.

Iyer, P. A. 1973 Instabilities in buoyancy driven buoyancy flows in a stably stratified medium. *Boundary Layer Met.* **5**, 53–66.

Iyer, P. A. & Kelly, R. E. 1978 Supercritical solutions for the buoyancy boundary layer. *J. Heat Transfer* **100**, 648–652.

Joseph, D. D. 1976 *Stability of Fluid Motions II*. Springer.

Kimura, S. & Bejan, A. 1984 The boundary layer natural convection regime in a rectangular cavity with uniform heat flux from the side. *J. Heat Transfer* **106**, 98–103.

Kolobkov, N. 1960 *Our Atmospheric Ocean*. Foreign Languages.

Kurtz, E. F. & Crandall, S. H. 1962 Computer-aided analysis of hydrodynamic stability. *J. Mathes Phys.* **41**, 264–279.

Laurie, D. P. 2001 Computation of Gauss-type quadrature formulas. *J. Comput. Appl. Math.* **127**, 201–217.

Levine, H. A. & Weinberger, H. F. 1986 Inequalities between Dirichlet and Neumann eigenvalues. *Arch. Rat. Mech. Anal.* **94** (3), 193–208.

Manins, P. C. & Sawford, B. L. 1979 A model of katabatic winds. *J. Atmos. Sci.* **36**, 619–630.

McBain, G. D. 2004 Skirting subsets of the plane, with application to marginal stability curves. *ANZIAM J.* **45(E)**, C78–C91.

McBain, G. D. & Armfield, S. W. 2004 Natural convection in a vertical slot: Accurate solution of the linear stability equations. *ANZIAM J.* **45(E)**, C92–C105.

Morley, A. 1954 *Strength of Materials*, 11th edn. Longmans, Green and Co.

Nachtsheim, P. R. 1963 Stability of free-convection boundary-layer flows. *Tech. Note* D-2089. NASA.

Peacock, T., Stocker, R. & Aristoff, J. M. 2004 An experimental investigation of the angular dependence of diffusion-driven flow. *Phys. Fluids* **16**, 3503–3505.

Phillips, O. M. 1970 On flows induced by diffusion in a stably stratified fluid. *Deep-Sea Res.* **17**, 435–440.

Plapp, J. E. 1957 The analytic study of laminar boundary-layer stability in free convection. *J. Aeronaut. Sci.* **24**, 318–319.

Polymeropoulos, C. E. & Gebhart, B. 1966 Stability of free convection flow over a vertical uniform flux plate. *AIAA J.* **4**, 2066–2068.

Prandtl, L. 1952 *Essentials of Fluid Dynamics*. Blackie.

Shapiro, A. & Fedorovich, E. 2004*a* Prandtl number dependence of unsteady natural convection along a vertical plate in a stably stratified fluid. *Intl J. Heat Mass Transfer* **47**, 4911–4927.

Shapiro, A. & Fedorovich, E. 2004*b* Unsteady convectively driven flow along a vertical plate immersed in a stably stratified fluid. *J. Fluid Mech.* **498**, 333–352.

Skyllingstad, E. D. 2003 Large-eddy simulation of katabatic flows. *Boundary Layer Met.* **106**, 217–243.

Stuart, J. T. 1958 On the non-linear mechanics of hydrodynamic stability. *J. Fluid Mech.* **4**, 1–21.

Szewcyzk, A. A. 1962 Stability and transition of the free-convection layer along a vertical flat plate. *Intl J. Heat Mass Transfer* **5**, 903–914.

Tao, J. 2006 Nonlinear global instability in buoyancy-driven boundary-layer flows. *J. Fluid Mech.* **566**, 377–388.

Tao, J., Le Quéré, P. & Xin, S. 2004*a* Absolute and convective instabilities of natural convection flow in boundary-layer regime. *Phys. Rev.* E **70**, 066311.

Tao, J., Le Quéré, P. & Xin, S. 2004*b* Spatio-temporal instability of the natural-convection boundary layer in thermally stratified medium. *J. Fluid Mech.* **518**, 363–379.

Villadsen, J. V. & Stewart, W. E. 1967 Solution of boundary-value problems by orthogonal collocation. *Chem. Engng Sci.* **22**, 1483–1501.

Weideman, J. A. C. & Reddy, S. C. 2000 A MATLAB differentiation matrix suite. *ACM Trans. Math. Software* **26**, 465–519.

Wunsch, C. 1970 On oceanic boundary mixing. *Deep-Sea Res.* **17**, 293–301.